Optical and dielectric properties of nitrophenolate based nonlinear optical crystal

**S. Dhanuskodi · A. Philominal · J. Philip ·
K. Kim · J. Yi**

Abstract A semi-organic nonlinear optical (NLO) material, lithium-*p*-nitrophenolate trihydrate (LPNP) was synthesized. Single crystals of dimensions $20 \times 7 \times 3$ mm^3 were harvested following the solvent evaporation technique. The functional groups present in the compound were identified from FT-IR and FT-Raman spectral analyses, and its molecular structure was confirmed. Identification of the compound was accomplished by X-ray diffraction technique (powder and single crystal XRD). The unit-cell dimensions and the morphology of the grown crystals were identified from single crystal XRD measurements. The thermal transport properties, thermal effusivity (*e*), thermal diffusivity (α), thermal conductivity (*k*) and heat capacity (*C*$_p$) were measured by the photopyroelectric technique at room temperature. Dielectric constant and dielectric loss were also measured as a function of frequency between 42 Hz and 5 MHz, and temperature between 32 and 100 °C. From optical transmittance measurements, the direct optical band gap of the LPNP crystal was estimated to be 2.47 eV. Laser damage threshold is 60.91 GW cm^{-2}. Powder second harmonic generation (SHG) measurement was carried out using a modified Kurtz–Perry technique. Third order nonlinear response was studied using Z-scan technique with a He–Ne laser (632.8 nm, 35 mW). The magnitude and the sign of the nonlinear absorption and nonlinear refraction are derived from a transmittance curve. The NLO parameters Intensity dependent refractive index n_2, nonlinear absorption coefficient β and third order susceptibility $\chi^{(3)}$ were estimated.

Introduction

Organic materials are emerging as alternatives to inorganic materials for nonlinear optical (NLO) applications because of their efficient molecular nonlinearity over a broad frequency range, low cost, low dielectric constants, inherent flexibility for synthesis, high optical damage threshold (>10 GW cm^{-2}), ultra-fast optical response coupled with efficient processing, and ease of fabrication and integration into devices. The molecular nonlinearity observed with the delocalized π electrons connected with donor–acceptor groups belonging to the organic ligand results in wide optical transmittance and high nonlinear electro-optic coefficients [1–3]. However, these crystals have certain limitations such as increased optical absorption and poor mechanical and thermal stability [4]. Metal complexes of thiourea, such as tristhiourea zinc sulphate (ZTS), bis(thiourea) cadmium chloride (BTCC) and bis(thiourea) zinc chloride (BTZC), L-arginine phosphate (LAP), L-arginine tetrafluoroborate, L-histidine tetrafluoroborate, etc., are some of the well-known semiorganic materials [5–7]. The organic ligand is ionically bonded to metal ion (or an inorganic host) to impart improved mechanical and thermal properties, which otherwise are lacking in organic materials. Lithium-*p*-nitrophenolate trihydrate (LPNP) is a semi-organic NLO material possessing large value for hyperpolarizability due to the presence of the organic

S. Dhanuskodi (✉) · A. Philominal
School of Physics, Bharathidasan University,
Tiruchirappalli 620024, India
e-mail: dhanus2k3@yahoo.com

J. Philip
Sophisticated Test and Instrumentation Centre, Cochin
University of Science and Technology, Cochin 682022, India

K. Kim · J. Yi
School of Information and Communication Engineering,
Sungkyunkwan University, 300, Chunchun-Dong,
Suwon 440-746, Korea

entity, *p*-nitrophenol. The organic ligand (nitrophenoxy), ionically bonded to the metal ion (lithium), along with intramolecular hydrogen bonding imparts high structural stability for this material. The crystal structure of the sodium analogue sodium-*p*-nitrophenolate (SPNP) was solved by Minemoto [8]. Crystal growth, topology and chemical etching properties of SPNP have been reported by Brahadeeswaran et al. [9]. The growth and characterization of the new semi-organic LPNP single crystal have been reported earlier [10]. The structural, microhardness and thermal properties of LPNP were reported by Milton Boaz et al. [11]. Dinakaran et al. [12] investigated the uniaxial growth of LPNP single crystal by Sankaranarayanan–Ramasamy [SR] method. In this work, we report the synthesis and characterization of LPNP, variation of its dielectric properties with frequency (range between 42 Hz and 5 MHz) and temperature (between 32 and 100 °C) as well as optical (linear and nonlinear) and thermal transport properties.

Experimental

Synthesis and crystal growth

LPNP was synthesized by dissolving *p*-nitrophenol and LiOH in the equimolar ratio in double distilled water at 32 °C. A yellow crystalline powder was obtained and it was further purified by re-crystallization process. LPNP possesses moderate solubility in water and hence it is a suitable solvent for the growth of good quality crystals. Yellow coloured single crystals were grown by slow evaporation technique, and crystals with the dimensions $20 \times 7 \times 3$ mm^3 were obtained over a period of 2 weeks. The photograph of a grown crystal and the morphology are shown in Fig. 1a and b for demonstration.

X-Ray diffraction techniques

The grown crystal was analyzed in a Four-circle Nonius CAD 4 MACH 3 single crystal X-ray diffractometer. Mo Kα radiation ($\lambda = 0.7071$ Å), made monochromatic with a graphite crystal, was used to identify the morphology and unit-cell parameters at 293 K.

The crystalline perfection of the grown single crystals was assessed by HRXRD by employing a multicrystal X-ray diffractometer developed at National Physical Laboratory, New Delhi. The well-collimated and monochromated MoKα$_1$ beam obtained from the three monochromator Si crystals set in dispersive $(+,-,-)$ configuration has been used as the exploring X-ray beam. The specimen crystal is aligned in the $(+,-,-,+)$ configuration.
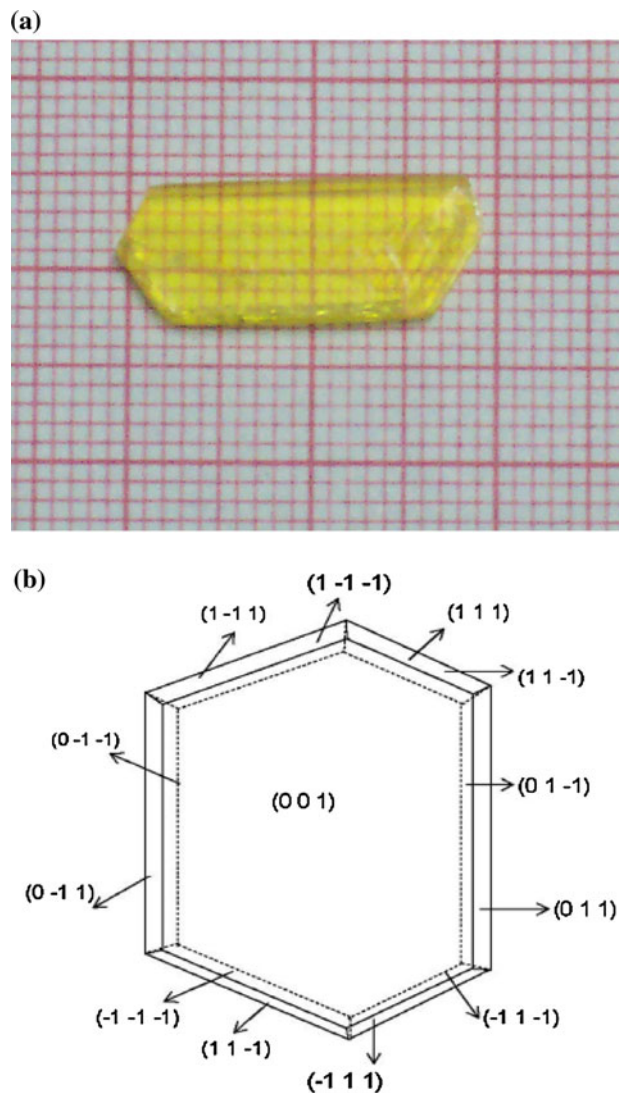
Fig. 1 a As grown single crystal of LPNP. **b** Morphology of LPNP crystal

FT-IR and FT-NMR techniques

The molecular structure of the synthesized compound was confirmed by FT-IR and FT-NMR analyses. FT-IR spectra of *p*-nitrophenol (PNP), SPNP and LPNP were recorded in the wavenumber range between 400 and 4000 cm^{-1} using a JASCO 460 PLUS FT-IR spectrometer at 25 °C following the KBr-pellet technique. FT-NMR spectra were recorded using a JEOL Model GSX 400, Bruker FT-NMR spectrometer 300 MHz with deuterated water used as the solvent.

Dielectric studies

Dielectric measurements on LPNP single crystal along the prominent (001) plane was carried out using a HIOKI 3532-50 LCR meter as a function of frequency between

42 Hz and 5 MHz and temperature between 32 and 100 °C. The two opposite flat faces of the crystal were coated with conductive silver paint to act as a capacitor with the crystal acting as the dielectric medium.

Photopyroelectric measurement

The photopyroelectric (PPE) technique has been employed to measure the thermal properties such as thermal effusivity, thermal diffusivity, thermal conductivity and specific heat capacity of this crystal [13]. A He–Cd laser beam (442 nm, 120 mW) modulated by a mechanical chopper is used as the optical heating source. A 28 μm thick film of polyvinylidene difluoride (PVDF) is used as the pyroelectric detector with pyroelectric coefficient $P = 0.25 \times 10^{-8}$ V cm^{-1} K^{-1} at room temperature. Measurements have been carried out for a crystal of thickness 1 mm normal to the prominent (001) plane. The generated thermal waves propagate through the sample and are detected by a pyroelectric detector. The output signal from the detector is measured with a lock-in amplifier.

Linear optical studies

The optical properties of a material are important as they provide information about the electronic structure, localized states and types of optical transitions [14]. Optical transmittance spectrum of LPNP crystal of thickness 1 mm has been recorded in the wavelength between 200 and 1380 nm using a Varian Cary 5E UV–Vis–NIR Spectrophotometer.

Laser induced surface damage threshold studies were performed using Q-switched Nd:YAG laser (1064 nm, 10 ns, 10 Hz). The laser beam was focused using a lens of focal length 20 cm and the measured focal spot size is 32.5 μm. The energy required to cause damage in the surface of the crystals of prominent plane (001) was measured using the power meter.

NLO studies

The second harmonic generation (SHG) efficiency of LPNP was measured by the modified Kurtz and Perry powder technique [15] using a Q-switched Nd:YAG laser ($\lambda = 1064$ nm, FWHM = 10 ns, PRF = 10 Hz and peak power = 3.3 mJ). All the crystalline samples were graded using standard sieves with the particle size ranges <106 μm, 106–125 μm, 125–150 μm and >150 μm for SHG measurements.

The third order NLO properties were estimated by Z-scan technique with a He–Ne laser (35 mW, 632.8 nm) with the sample thickness 1 mm. In this method the sample is translated in the Z-direction along the axis of a focussed

Gaussian beam and the far field intensity is measured as a function of the sample position. A spatial distribution of the temperature in the crystal surface is produced due to the localized absorption of a tightly focused beam propagating through the absorbing crystal. Hence the spatial variation of the refractive index is produced, which acts as a thermal lens resulting in the phase distortion of the propagating beam. The difference between the peak and valley transmission (ΔT_{p-v}) is written in terms of the on-axis phase shift |$\Delta \phi_o$| at the focus. The experimental data were theoretically fitted with an equation described by Sheik-Bahae et al. [16]. The normalized transmission for the closed aperture condition is given by

$$T(x) = 1 - \frac{4x\Delta\phi_0}{(x^2 + 9)(x^2 + 1)}, \tag{1}$$

where

$$\Delta\phi_0 = \frac{\Delta T_{p-v}}{0.406(1 - S)^{0.25}}, \tag{2}$$

and the normalized transmission for the open aperture condition is

$$T(z) = 1 - q_0/2\sqrt{2} \quad \text{for } q_0 < 1, \tag{3}$$

where

$$q_0(z) = \beta I_0 L_{eff}/[1 + (z/z_0)]^2. \tag{4}$$

Here β is the nonlinear absorption coefficient, I_0 is the irradiance at the focus, L_{eff} is the effective length of the sample, z is the position of the sample and z_0 is the Rayleigh range of the lens.

Results and discussion

Structural analyses

LPNP crystallizes into the monoclinic system with space group Pa. The crystal has a total eight faces, among which four are unique and the other four have their friedal parallels. Among the eight faces, the crystal has one prominent flat face indexed as (001) and the other flat faces are (0−11), (1−11) and (111). Since $\beta = 90.604°$, c and c^* directions are almost coincident with each other. The shortest growth direction is along c, which is the largest unit-cell axis. The unit-cell parameters of LPNP single crystal are found to be, $a = 10.838(8)$ Å, $b = 7.519(4)$ Å, $c = 11.361(4)$ Å and $V = 925.7(9)$ Å^3. The density ρ of the crystal was theoretically calculated using crystallographic data as 1.379 gm cm^{-3} and verified by floatation method as 1.378 gm cm^{-3}. Figure 2 shows the high-resolution diffraction curve (DC) recorded for the grown LPNP single crystal using (001) diffracting planes in symmetrical
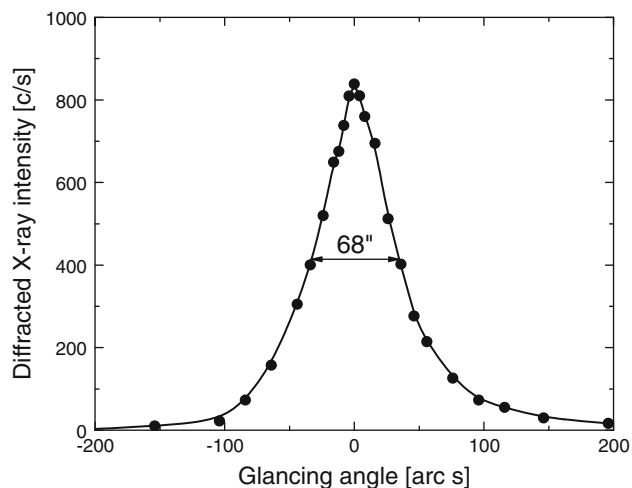
Fig. 2 High-resolution X-ray diffraction curve [(001) planes, MoKα₁, (+,−,−,+)]

Bragg geometry by employing the multicrystal X-ray diffractometer with MoKα₁ radiation. The DC contains a single peak and indicates that the specimen is free from structural grain boundaries.

The FWHM of the curve is 68 arcs, which is somewhat more than that expected from the plane-wave theory of dynamical X-ray diffraction, for an ideally perfect crystal but close to that expected for nearly perfect real-life crystals. This much broadness with good scattered intensity along the wings/tails of the DC indicates that the crystal contains both vacancy and interstitial type of defects with considerable density. Such defects are very common to observe in almost all real crystals including nature gifted crystals and are many times unavoidable due to thermodynamical conditions.

A weak absorption in the IR spectrum in the region 1584–1664 cm^{-1} confirms the presence of phenolic ring [17]. The absorptions in the lower frequency region (400–500 cm^{-1}) are due to the overtones of the fundamental vibrations of *p*-nitrophenolates. A broad intermolecular H-bonded O–H symmetric stretching at 3331 cm^{-1} of *p*-nitrophenol is shifted to high frequencies 3406 and 3366 cm^{-1}, respectively, for LPNP and SPNP. This shift increases the polarizability of *p*-nitrophenol to a higher order and it easily forms a metal coordination (Li/Na) compound and hence confirms the molecular structure.

The proton–carbon configurations of the synthesized compound have been elucidated by ^{1}H and ^{13}C NMR spectroscopy. From the spectra it is observed that the signals at $\delta = 6.457$ ppm and $\delta = 7.994$ ppm (doublet of doublet) confirm the presence of chemically equivalent protons attached to the aromatic ring. A singlet at $\delta = 4.668$ ppm indicates the presence of two protons in the water molecule. The carbon present in the phenolic ring

was confirmed from the ^{13}C NMR spectrum. The absorption peaks at $\delta = 119.24$ ppm and $\delta = 128.13$ ppm show the chemically equivalent aromatic carbons (C=C). The chemical shift at $\delta = 177.88$ ppm is due to the nitro carbon of LPNP. The shift at 134 ppm identifies the protonation site of LPNP.

Dielectric analysis

From the dielectric measurement, the capacitance of parallel plate capacitor as a function of frequency and temperature was measured. The dielectric constant ε' and dielectric loss ε'' were calculated. Plots of ε' and ε'' against log (frequency) at different temperatures are shown in Fig. 3a and b.

From the dielectric constant profiles, shown in Fig. 3a and b, it is evident that the dielectric constant decreases with increasing frequency and increases with increasing temperature. The increase in dielectric constant at low frequencies are attributed to the dependance of space charge polarization and the increase in dielectric constant
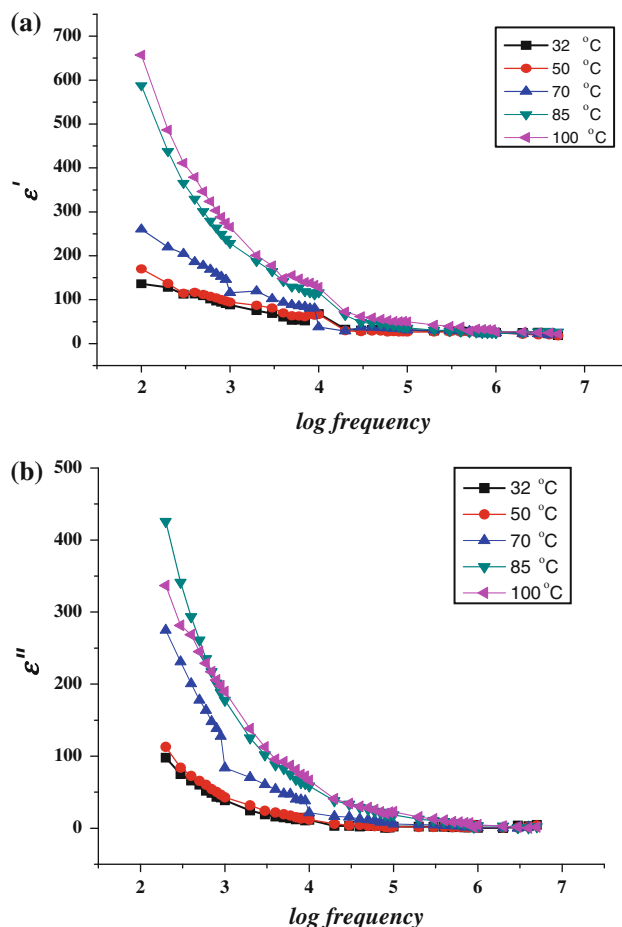
Fig. 3 Variation of **a** ε' and **b** ε'' with log (frequency) at different temperatures

Table 1 Comparison of thermal parameters of some of the nonlinear optical crystals [21]

| System	Thermal diffusivity (α) (10^{-7} m^2 s^{-1})	Thermal effusivity (e) (J m^{-2} K^{-1} s$^{-1/2}$)	Heat capacity (C_p) (J Kg^{-1} K^{-1})	Thermal conductivity (k) (W m^{-1} K^{-1})
*LPNP	90.02	308.02	790.2	9.24
PPNP	22.5	682	276	1.02
2A5NPFB	98.2	171	30	0.53
EDMP·3H$_2$O	17.44	661.4	716.1	0.873
MDMP·3H$_2$O	18.04	663.6	706.4	0.891
KDP			857 (298 K)	1.21 (302 K)

with increasing temperature leads to the conclusion that thermal excitations of atoms about their lattice points results in disordering the lattice [18]. Here the space charge contribution to polarization is due to the purity of the material. Dielectric constants at low frequency are comparable to optical frequencies, which lead to minimization of the phase mismatch between optical and electrical pulses in high-speed travelling wave devices. In accordance with the Miller Rule, the lower value of dielectric constant at high frequencies is a suitable parameter for the enhancement of SHG coefficient [19]. The variation of dielectric loss as a function of frequency and temperature follows the same trend as that of the dielectric constant. From the profile, it is observed that the higher loss at higher temperatures and at lower frequencies may be due to space charge and macroscopic distortion [20]. Also the hopping of the charge carriers in the lattice sites is thermally activated by an increase in the temperature.

Thermal properties

Measurement of the PPE phase and amplitude enables one to determine the thermal diffusivity (α) and thermal effusivity (e). From the measured values of α and e, thermal conductivity (k) and heat capacity (C_p) are calculated. Table 1 presents the comparison of thermal parameters of some of the other well-known NLO crystals [21]. The thermal conductivity and heat capacity of LPNP is found to be high (comparable to KDP and KN) among the reported NLO crystals. Since these factors have an impact on conversion efficiencies, it is necessary to find the structural relationship between them. It means that, higher the heat capacity larger the SHG efficiency. This accounts the possibility of occurrence of larger laser induced surface damage threshold in the crystals.

Optical properties

The lower cutoff wavelength is 450 nm and a transparency around 80% in the wavelength range 450–1380 nm suggests its suitability for the generation of second harmonics
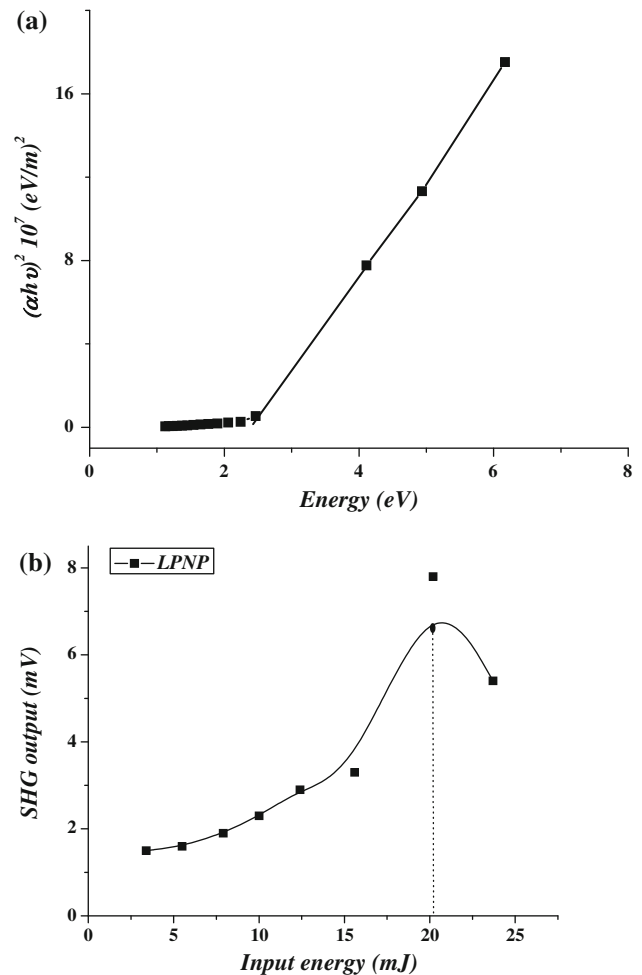
Fig. 4 **a** Variation of $(\alpha h\nu)^2$ with photon energy. **b** Variation of SHG output against input energy

with IR radiation from an Nd:YAG laser. The dependence of optical absorption coefficient on photon energy helps to understand the band structure and type of transitions that electrons undergo [22]. The optical energy gap is determined from the spectral dependence of the absorption coefficient (α), which is written as a function of photon energy $h\nu$ as [23]
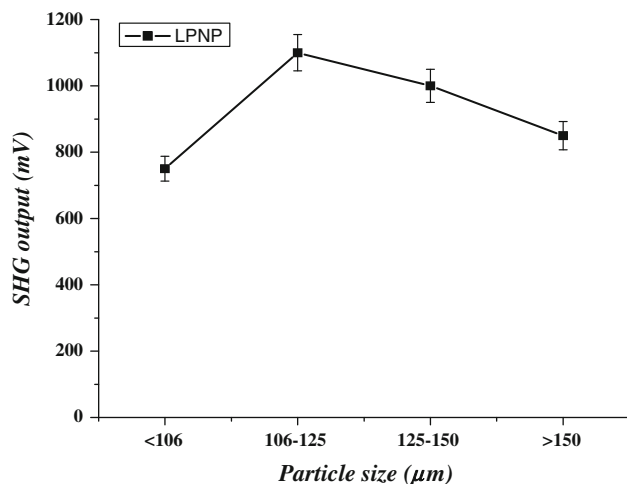
Fig. 5 Variation of SHG output with particle size

$$\alpha h v^2 = A \left(E_g - h v \right) \tag{5}$$

where E_g is the optical band gap and A is a constant. The variation of $(\alpha h v)^2$ with photon energy has been plotted, as shown in Fig. 4a, from which the value of direct energy band gap E_g is estimated as 2.47 eV. By Brewster's Method, using He–Ne laser ($\lambda = 632.8$ nm, 10 mW) the linear refractive index was found to be 1.38 ± 0.13.

Graph was plotted SHG output (mV) against input energy (mJ) of the beam (Fig. 4b). It is inferred that, the SHG output is increased on increasing the input energy and reaches maximum until damage occurs and decreases with further increase of input energy. Here the maximum energy was taken for the calculation. Thus the surface damage threshold of the LPNP crystal is calculated using the relation,

$$\text{Power density}(P) = \frac{E}{\tau \pi \omega^2} \tag{6}$$

where E is the input energy (mJ), τ is the pulse width (ns) and ω is the radius of the spot (μm). The surface damage threshold of the LPNP crystal is found to be 60.91 GW cm^{-2}. The dispersion of heat induced by the absorption of the laser radiation in the material strongly depends on the thermal diffusivity which leads to the occurrence of damage in crystals. As expected that, higher

the heat capacity and larger is the laser induced surface damage threshold.

The variation of SHG output with particle size is shown in Fig. 5. The relative powder SHG efficiency for the average particles size is found to be 9.25 times of KDP. It is noted that the SHG output initially increases and then decreases with further increase of particle size. This confirms the non phase matchable behaviour of the material. The higher is the SHG efficiency of the material the better it is for NLO applications.

A theoretical fit of Eqs. 3 and 4 to the closed and open aperture yields values for the nonlinear refraction (n_2) and nonlinear absorption (β) (Table 2). Figure 6a and b shows the normalized transmission (normalized to the linear transmittance of the sample) of the closed and open aperture Z-scan of LPNP single crystal. The enhanced transmission near the focus is suggestive of the saturation of the absorption at high intensity. The self defocusing effect is due to thermal nonlinearity results in the absorption of radiation at 632.8 nm [24, 25]. The results of Z-scan for LPNP single crystal are given below.

The typical peak–valley transmittance curve is obtained when the nonlinear refractive index of the medium is negative. The nonlinear absorption can be ascribed to saturable absorption and the nonlinear refraction leads to the self defocusing in the crystal. The peak–valley pattern of the transmittance curve obtained under the closed aperture configuration shows the characteristic self defocusing behaviour of the propagation of the laser beam in the sample. The value of (χ^3) under same condition is comparable to that of well-known NLO materials like ZTS [26], organic dye [24] and triphenylmethane [27] are $3.5 \pm 0.17 \times 10^{-4}$ esu, 7.24×10^{-6} esu and 8.37×10^{-6} esu, respectively.

Conclusions

A semi-organic NLO material, LPNP was synthesized and single crystals were grown by slow evaporation technique. The molecular structure was confirmed by the FT-IR and FT-Raman techniques and the unit-cell dimensions were determined by powder and single crystal X-ray diffraction

Table 2 The results of Z-scan for LPNP single crystal		
Linear refractive index n (Brewster's method)		1.38 ± 0.13
Nonlinear refractive index (n_2)		$(-3.44 \pm 0.17) \times 10^{-12}$ cm^2 W^{-1}
Nonlinear absorption coefficient (β)		$(-2.17 \pm 0.11) \times 10^{-4}$ cm W^{-1}
Real part of the third order susceptibility [Re(χ^3)]		$(-1.66 \pm 0.08) \times 10^{-10}$ esu [-2.32×10^{-18} (m/s)$^{-2}$]
Imaginary part of the third order susceptibility [Im(χ^3)]		$(-5.3 \pm 0.26) \times 10^{-8}$ esu [-7.4×10^{-16} (m/s)$^{-2}$]
Third order nonlinear susceptibility (χ^3)		$(5.3 \pm 0.26) \times 10^{-8}$ esu [7.4×10^{-16} (m/s)$^{-2}$]
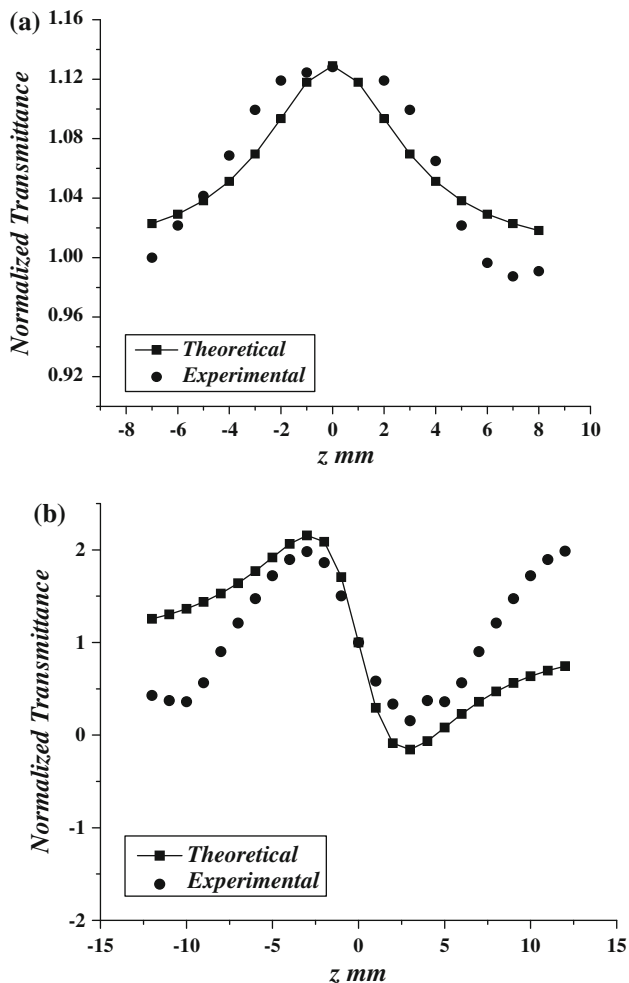
Fig. 6 Normalized transmission for **a** *open* and **b** *closed* aperture Z-scan

analyses. The proton and carbon configurations were elucidated from the FT-NMR spectra. The thermal parameters α, e, k, C_p were determined by photopyroelectric measurements at room temperature. It is found that the values of k and C_p are comparable to inorganic $KNbO_3$ and organic 1-ethyl-2,6-dimethyl-4(1H)-pyridinone trihydrate (EDMP). It shows the powder SHG efficiency for the average particle size of about 9.25 times higher than KDP. The dielectric constant of the crystal at room temperature is 18, which remains invariant at higher frequencies. From the optical transmittance measurements, the lower cutoff wavelength is obtained as 450 nm and the optical transmittance window as 450–1380 nm. Transparency is obtained as 80% and the optical direct band gap as 2.47 eV. Laser damage threshold of LPNP crystal is found to be 60.91 GW cm^{-2}. The nonlinear absorption is due to

the saturable absorption while the nonlinear refraction leads to self defocusing. Thus the LPNP crystal is a promising candidate to make efficient light emitting diodes working in the visible region.

References

1. Dehu C, Meyers F, Bredas JL (1993) J Am Chem Soc 115:6198
2. Rosker MJ, Marcy HO (1997) Novel optical materials and applications. Wiley, New York
3. Milton Boaz B, Mary Navis Priya S, Mary Linet J, Martin Deva Prasath P, Jerome Das S (2007) Opt Mater 29:827
4. Brahadeeswaran S, Bhat HL, Kini NS, Umarji AM, Balaya P, Goyal PS (2000) J Appl Phys 88:5935
5. Dhanuskodi S, Pricilla Jeyakumari A, Manivannan S (2005) J Cryst Growth 282:72
6. Angeli Mary PA, Dhanuskodi S (2001) Spectrochim Acta A 57:2345
7. Ramajothi J, Dhanuskodi S (2003) Cryst Res Technol 38:986
8. Minemoto H, Sonoda N, Miki K (1992) Acta Cryst C48:737
9. Brahadeeswaran S, Venkatraman V, Sherwood JN, Bhat HL (1998) J Mater Chem 8:613
10. Milton Boaz B, Rajesh AL, Xavier Jesu Raja S, Jerome Das S (2004) J Cryst Growth 262:531
11. Milton Boaz B, Santhana Raman P, Xavier Jesu Raja S, Jerome Das S (2005) Mater Chem Phys 93:187
12. Dinakaran S, Jerome Das S (2008) J Cryst Growth 310:410
13. Preethy Menon C, Philip J (2000) Meas Sci Technol 11:1744
14. Anie Roshan S, Joseph C, Ittyachan MA (2001) Mater Lett 49:299
15. Kurtz SK, Perry TT (1968) J Appl Phys 39:3798
16. Sheik-Bahae M, Said AA, Wei J-H, Hagan DJ, Vanstryland EW (1990) IEEE J Quantum Electron 26:760
17. Robert Silverstein M, Francis Webster X (2003) Spectroscopic identification of organic compounds, 6th edn. Wiley, Asia
18. Arora SK, Patil V, Amin B, Kothari A (2004) Bull Mater Sci 27:141
19. Miller RC (1964) Appl Phys Lett 5:17
20. Hinano S, Kim PC, Orihara H, Umeda, Ishibasi Y (1990) J Mater Sci 25:2800. doi:10.1007/BF00584883
21. Manivannan S, Dhanuskodi S, Tiwari SK, Philip J (2008) Appl Phys B 90:489
22. Periasamy BK, Jebas RS, Gopalakrishnan N, Balasubramanian T (2007) Mater Lett 61:4246
23. Yakuphanoglu F, Cukurovali A, Yilmaz I (2004) Physica B 351:53
24. Mohammed Ali Q, Palanisamy PK (2005) Optik 116:515
25. Sheik-Bahae M, Hutchings DC, Hagan DJ, Vanstryland EW (1991) IEEE J Quantum Electron 27:1296
26. Sabari Girisun TC, Dhanuskodi S (2009) Cryst Res Technol 44:1
27. Geethakrishnan T, Palanisamy PK (2007) Opt Commun 270:424